J. Fluid Mech. (2013), *vol.* 729, *pp.* 285–308.
doi:10.1017/jfm.2013.278

Low-dimensional modelling of high-Reynolds-number shear flows incorporating constraints from the Navier–Stokes equation

Maciej J. Balajewicz[1],†, Earl H. Dowell[2] and Bernd R. Noack[3]

[1]Department of Aeronautics and Astronautics, Stanford University, Stanford, CA 94305, USA

[2]Department of Mechanical Engineering and Materials Science, Duke University, Durham, NC 27708, USA

[3]Institut PPRIME, CNRS – Université de Poitiers – ENSMA, UPR 3346, Département Fluides, Thermique, Combustion, CEAT, 43 rue de l'Aérodrome, F-86036 POITIERS CEDEX, France

(Received 8 November 2012; revised 8 November 2012; accepted 25 May 2013)

We generalize the POD-based Galerkin method for post-transient flow data by incorporating Navier–Stokes equation constraints. In this method, the derived Galerkin expansion minimizes the residual like POD, but with the power balance equation for the resolved turbulent kinetic energy as an additional optimization constraint. Thus, the projection of the Navier–Stokes equation on to the expansion modes yields a Galerkin system that respects the power balance on the attractor. The resulting dynamical system requires no stabilizing eddy-viscosity term – contrary to other POD models of high-Reynolds-number flows. The proposed Galerkin method is illustrated with two test cases: two-dimensional flow inside a square lid-driven cavity and a two-dimensional mixing layer. Generalizations for more Navier–Stokes constraints, e.g. Reynolds equations, can be achieved in straightforward variation of the presented results.

Key words: computational methods, low-dimensional models, turbulence modelling

1. Introduction

Numerical simulation of fluid flows can be a very computationally intensive endeavour. In addition, reaching a physical understanding from numerical simulation data can provide another challenge. Both challenges are partially addressed by model order reduction (MOR) techniques capable of producing reduced-order models (ROMs) of complex fluid flows that retain some physical fidelity while substantially reducing the size and cost of the computational model.

In fluid flow applications, proper orthogonal decomposition (POD) and Galerkin projection form a popular MOR strategy (Noack, Morzynski & Tadmor 2011; Holmes *et al.* 2012). However, the development of robust and accurate ROMs using the

† Email address for correspondence: maciej.balajewicz@stanford.edu

POD–Galerkin method for turbulent fluid flows remains an active area of research. Turbulence is a phenomenon characterized by chaotic, multi-scale dynamics, in both space and time. At high Reynolds numbers, the dynamics of turbulence exhibit an energy cascade: large-scale eddies are broken down into smaller and smaller eddies until the scales are fine enough so that viscous forces can dissipate their energy (Tennekes & Lumley 1972; Moin & Mahesh 1998; Pope 2000). Application of the standard POD–Galerkin method to a turbulent flow needs to account for this energy cascade. On a kinematic level, POD, by construction, is biased towards the large, energy-producing scales of the turbulent flow. Hence, on a dynamic level, straightforward Galerkin projection yields ROMs that are not endowed with the natural energy dissipation of the small dissipative scales. In principle, the problem can be cured by direct modelling of small-scale dynamics by inclusion of a sufficiently large number of POD modes. However, this will lead to ROMs that may quickly become more expensive then the computational fluid dynamics solver used to create the snapshots. In practice, the unresolved small-scale dissipation is accounted for by an additional empirical subgrid-turbulence term. Unfortunately, this approach may affect the ROM solution in undesirable ways, as these auxiliary terms modify the Galerkin system dynamics (Aubry *et al.* 1988; Rempfer & Fasel 1994; Ukeiley *et al.* 2001; Sirisup & Karniadakis 2004; Bailon-Cuba *et al.* 2012; Iliescu & Wang 2012).

In this paper, an alternative strategy to MOR of turbulent flows is proposed. Some of the energy-dissipative small scales are absorbed into the Galerkin expansion modes – instead of accounting for these unresolved small scales with empirical eddy-viscosity terms on the Galerkin system level. In particular, the proposed generalization of the POD modes is guaranteed to respect the power balance equation for the resolved turbulent kinetic energy. Thus, the projection on to the new expansion modes yields adequate Galerkin systems without auxiliary eddy-viscosity terms. The proposed methodology is formulated as a small-scale constrained minimization problem that can be solved numerically using standard, off-the-shelf MATLAB algorithms.

This paper is organized as follows. In § 2, the POD and Galerkin methods are summarized for the incompressible Navier–Stokes equation. In § 3, the proposed new approach is introduced and the algorithm and its numerical implementation are outlined. In § 4, two classical benchmarks, the lid-driven cavity and a mixing layer, are modelled using the standard POD–Galerkin approach and the new approach. Finally, in § 5, the main results are summarized and future prospects laid out.

2. Traditional Galerkin method

We recapitulate the traditional Galerkin method with orthonormal global modes as a starting point for our innovation in § 3.

2.1. *Spectral method*

Consider a dynamical system that evolves in a Hilbert space H, $\boldsymbol{u}(t) \in H$, governed by

$$\frac{\mathrm{d}}{\mathrm{d}t}\boldsymbol{u} = \boldsymbol{F}(\boldsymbol{u}), \tag{2.1}$$

where $\boldsymbol{F}$ is the propagator in H. In fluid flows, the state variable $\boldsymbol{u} = \boldsymbol{u}(\boldsymbol{x}, t)$ depends on space $\boldsymbol{x} \in \Omega, \Omega$ being the flow domain, and time $t \in [0, T], T$ representing

the period of integration. Then, the propagator $\boldsymbol{F}$ contains spatial derivatives. The associated Hilbert space of square-integrable functions $L^2(\Omega)$ is equipped with the standard inner product for its elements $\boldsymbol{u}, \boldsymbol{v} \in L^2(\Omega)$,

$$(\boldsymbol{u}, \boldsymbol{v})_\Omega := \int_\Omega \boldsymbol{u} \cdot \boldsymbol{v} \, \mathrm{d}\boldsymbol{x}, \tag{2.2}$$

where ':=' defines the left-hand side in terms of the right-hand side.

In the spectral approach (Canuto *et al.* 1991, 2006; Boyd 2001), the governing variable, $\boldsymbol{u}(\boldsymbol{x}, t)$ is discretized using basis functions (modes) $\{\boldsymbol{u}_i(\boldsymbol{x})\}_{i=1}^{\infty} \in H$ with corresponding mode coefficients $\{a_i(t)\}_{i=1}^{\infty}$:

$$\boldsymbol{u}(\boldsymbol{x}, t) \approx \boldsymbol{u}^{[1..n]}(\boldsymbol{x}, t) := \sum_{i=1}^{n} a_i(t) \, \boldsymbol{u}_i(\boldsymbol{x}). \tag{2.3}$$

In the method of lines, the modes $\boldsymbol{u}_i$ are known *a priori* and the goal is to find mode coefficients a_i that satisfy the differential equation. In general, the origin and form of the modes $\boldsymbol{u}_i$ can be arbitrarily chosen. In the context of spectral methods in computational fluid dynamics (CFD), the spatial basis functions, $\boldsymbol{u}_i$ are usually analytical functions, e.g. trigonometric functions or Chebyshev polynomials. The advantage of these functions is that their spatial derivatives have analytical representations and numerically efficient algorithms such as the fast Fourier transform (FFT) can be utilized. In the context of MOR, the spatial basis functions may be derived *a priori* using completeness conditions (Ladyzhenskaya 1963; Noack & Eckelmann 1994), from Navier–Stokes eigenfunctions (Joseph 1976), or *a posteriori* from a snapshot of a solution dataset, such as the proper orthogonal decomposition (POD) (Holmes *et al.* 2012) or dynamic mode decomposition (DMD) (Rowley *et al.* 2009; Schmid 2010).

The mode coefficients a_i are chosen to minimize the residual of the Galerkin expansion. Let $\{\boldsymbol{v}_i \in H \mid i = 1, \ldots, n\}$ be a basis for a subspace of H. We seek a_i such that

$$\left(\boldsymbol{v}_i, \frac{\mathrm{d}}{\mathrm{d}t}\boldsymbol{u}^{[1..n]}\right)_\Omega - \left(\boldsymbol{v}_i, \boldsymbol{F}\left(\boldsymbol{u}^{[1..n]}\right)\right)_\Omega = 0. \tag{2.4}$$

In the traditional Galerkin method, the trial basis is equal to the test basis; $\boldsymbol{v}_i \equiv \boldsymbol{u}_i$ (Fletcher 1984). The projection yields a set of evolution equations for the mode coefficients a_i:

$$\frac{\mathrm{d}}{\mathrm{d}t} a_i = f_i(\boldsymbol{a}), \tag{2.5}$$

where $\boldsymbol{a} := (a_1, \ldots, a_n)^{\mathrm{T}}$ represents the state and $\boldsymbol{f} := (f_1, \ldots, a_n)^{\mathrm{T}}$ its propagator. Given the initial conditions, the evolution equation can be integrated using standard numerical integration techniques.

2.2. *Proper orthogonal decomposition (POD)*

We express the POD optimality condition in terms of the instantaneous turbulent kinetic energy $E(t)$ of the flow, defined as

$$E(t) := \frac{1}{2} \int_\Omega |\boldsymbol{u}(\boldsymbol{x}, t) - \boldsymbol{u}_0(\boldsymbol{x})|^2 \, \mathrm{d}\boldsymbol{x}. \tag{2.6}$$

POD provides an expansion that minimizes its averaged residual in the energy norm. As a consequence, the instantaneous turbulent kinetic energy of the expansion

$$E^{[1..n]}(t) := \frac{1}{2}\int_\Omega \left|\sum_{i=1}^{n} a_i(t)\boldsymbol{u}_i(\boldsymbol{x})\right|^2 \mathrm{d}\boldsymbol{x} \tag{2.7}$$

is as close as possible, on average, to the corresponding energy of the employed flow data. The average of a state variable F in the data horizon $[0, T]$ and is defined by

$$\langle F\rangle_T := \frac{1}{T}\int_0^{\mathrm{T}} F\,\mathrm{d}t. \tag{2.8}$$

The optimality condition for POD can be formulated as follows:

$$\begin{aligned} \underset{\boldsymbol{a},\boldsymbol{u}_i}{\arg\min} \quad & \left\langle \int_\Omega \left|\boldsymbol{u}(\boldsymbol{x},t) - \boldsymbol{u}_0(\boldsymbol{x}) - \sum_{i=1}^{n} a_i(t)\boldsymbol{u}_i(\boldsymbol{x})\right|^2 \mathrm{d}\boldsymbol{x}\right\rangle_T \\ \text{s.t.} \quad & \left(\boldsymbol{u}_i, \boldsymbol{u}_j\right)_\Omega = \int_\Omega \boldsymbol{u}_i(\boldsymbol{x})\cdot\boldsymbol{u}_j(\boldsymbol{x})\,\mathrm{d}\boldsymbol{x} = \delta_{ij}, \end{aligned} \tag{2.9}$$

where δ_{ij} is the Kronecker delta function. For later reference, we lump the second moments of the mode coefficients into a $n \times n$ correlation matrix:

$$\boldsymbol{\Lambda} := \left(\lambda_{ij}\right) \quad \text{where } \lambda_{ij} := \langle a_i, a_j\rangle_T. \tag{2.10}$$

Note that $\boldsymbol{\Lambda}$ is a diagonal matrix, $\lambda_{ij} = \delta_{ij}\lambda_i$ where the diagonal term λ_i represents the ith POD eigenvalue. The discretized equivalent of (2.9) is solved using the well-known Eckart–Young theorem (Demmel 1997) of singular value decomposition (SVD) and the method of snapshots (Sirovich 1987).

2.3. *Galerkin MOR of the Navier–Stokes equation*

The evolution of the velocity field $\boldsymbol{u}(\boldsymbol{x}, t)$ of an incompressible Newtonian fluid is governed by the equation of continuity and the Navier–Stokes equation

$$\nabla\cdot\boldsymbol{u} = 0, \tag{2.11a}$$

$$\frac{\partial\boldsymbol{u}}{\partial t} = \nu\Delta\boldsymbol{u} - \nabla\cdot(\boldsymbol{u}\boldsymbol{u}) - \nabla p, \tag{2.11b}$$

where ν is the viscosity and p is the pressure. The flow is described in a steady domain Ω, with a Dirichlet, free stream or convective outflow condition on the boundary $\partial\Omega$. We augment the Galerkin expansion (2.21) with the basic mode $\boldsymbol{u}_0$ as temporal mean flow:

$$\boldsymbol{u}(\boldsymbol{x},t) \approx \boldsymbol{u}^{[0..n]}(\boldsymbol{x},t) := \boldsymbol{u}_0(\boldsymbol{x}) + \sum_{i=1}^{n} a_i(t)\boldsymbol{u}_i(\boldsymbol{x}). \tag{2.12}$$

The basic mode satisfies the original boundary conditions while the modes respect the homogenized version. Thus, the Galerkin expansion (2.12) fulfils the boundary conditions for all choices of mode coefficients a_i. In addition, the equation of continuity (2.11a) is satisfied for all choices of mode coefficients by the solenoidal

modes $\nabla \cdot \boldsymbol{u}_i = 0, i = 0, \ldots, n$. Galerkin projection on (2.11*b*) yields a set of n coupled, quadratic ordinary differential equations (ODEs):

$$\frac{\mathrm{d}}{\mathrm{d}t} a_i = C_i + \sum_{j=1}^{n} L_{ij} a_j + \sum_{j,k=1}^{n} Q_{ijk} a_j a_k. \tag{2.13}$$

For the sake of brevity, dependence on time and space is omitted in the remaining part of this paper. For the assumed divergence-free spatial basis functions and boundary conditions, the Galerkin system coefficients read as follows:

$$C_i = \nu(\boldsymbol{u}_i, \Delta \boldsymbol{u}_0)_{\Omega} - (\boldsymbol{u}_i, \nabla \cdot (\boldsymbol{u}_0 \boldsymbol{u}_0))_{\Omega}, \tag{2.14a}$$

$$L_{ij} = \nu\big(\boldsymbol{u}_i, \Delta \boldsymbol{u}_j\big)_{\Omega} - \big(\boldsymbol{u}_i, \nabla \cdot (\boldsymbol{u}_0 \boldsymbol{u}_j)\big)_{\Omega} - \big(\boldsymbol{u}_i, \nabla \cdot (\boldsymbol{u}_j \boldsymbol{u}_0)\big)_{\Omega}, \tag{2.14b}$$

$$Q_{ijk} = -\big(\boldsymbol{u}_i, \nabla \cdot (\boldsymbol{u}_j \boldsymbol{u}_k)\big)_{\Omega}. \tag{2.14c}$$

For open flows, the Galerkin pressure-term representation does not vanish identically and leads to contributions to all coefficients C_i, L_{ij} and Q_{ijk} (Noack, Papas & Monkewitz 2005). In practice, however, the pressure term is either neglected or modelled well using a linear fit of the linear Galerkin term L_{ij} (Galletti *et al.* 2004; Noack *et al.* 2005).

2.4. *Power balance*

In this section, we revisit the power balance in the Galerkin subspace to motivate the proposed innovation of the next section. For a statistically stationary turbulent flow, the total power of turbulent kinetic energy vanishes on average, i.e. $\langle (\mathrm{d}/\mathrm{d}t) E \rangle_T = 0$. This is also true in the subspace spanned by the first n POD modes. The instantaneous energy in this Galerkin space is given exactly by

$$E^{[1..n]} := \frac{1}{2} \sum_{i=1}^{n} a_i^2. \tag{2.15}$$

The rate of change, called the *(total) power* in the sequel, reads as follows:

$$\frac{\mathrm{d}}{\mathrm{d}t} E^{[1..n]} := \sum_{i=1}^{n} a_i \frac{\mathrm{d}}{\mathrm{d}t} a_i. \tag{2.16}$$

The exact derivative of the mode coefficients requires the interactions with the complete set of POD modes:

$$\frac{\mathrm{d}}{\mathrm{d}t} a_i = C_i + \sum_{j=1}^{\infty} L_{ij} a_j + \sum_{j,k=1}^{\infty} Q_{ijk} a_j a_k. \tag{2.17}$$

Thus, (2.16) becomes

$$\frac{\mathrm{d}}{\mathrm{d}t} E^{[1..n]} = \sum_{i=1}^{n} C_i a_i + \sum_{i=1}^{n} \sum_{j=1}^{\infty} L_{ij} a_i a_j + \sum_{i=1}^{n} \sum_{j,k=1}^{\infty} Q_{ijk} a_i a_j a_k. \tag{2.18}$$

The averaged total power (2.18) has to vanish. The resulting power balance is simplified by employing the POD coefficient statistics $\langle a_i \rangle_T = 0$, $\langle a_i a_j \rangle_T = \delta_{ij}\lambda_j$:

$$0 = \left\langle \frac{\mathrm{d}}{\mathrm{d}t} E^{[1..n]} \right\rangle_T = \sum_{i=1}^{n} L_{ii}\lambda_i + \sum_{i=1}^{n}\sum_{j,k=1}^{\infty} Q_{ijk}\langle a_i a_j a_k \rangle_T. \tag{2.19}$$

Additional insights can be gained from employing energy preservation of the quadratic term $Q_{ijk} + Q_{ikj} + Q_{jik} + Q_{jki} + Q_{kij} + Q_{kji} = 0$ (Kraichnan & Chen 1989). This energy preservation annihilates all triads resolved in the considered POD space, i.e. $Q_{ijk}\langle a_i a_j a_k \rangle_T$, $i, j, k = 1, \ldots, n$. The resulting total power balance contains the resolved linear term $\sum_{i=1..n} L_{ii}\lambda_i$, comprising production, convection and dissipation (Noack *et al.* 2005) and the unresolved transfer term $T_< := \sum_{i=1}^{n}\sum_{\substack{j,k=1 \\ \max(j,k)>n}}^{\infty} Q_{ijk}\langle a_i a_j a_k \rangle_T$ (Holmes *et al.* 2012):

$$0 = \sum_{i=1}^{n} L_{ii}\lambda_i + T_<. \tag{2.20}$$

The unresolved transfer term $T_<$ describes the nonlinear energy transfer from resolved large-scale modes to neglected higher-order small-scale modes and is generally negative. This means that the Galerkin system with n POD modes must be expected to predict an excess unresolved power $\sum_{i=1}^{n} L_{ii}\lambda_i$ on the Navier–Stokes attractor and as a result over-predict the fluctuation level. This excess resolved power can absorbed by an eddy-viscosity model, i.e. by an additional term in the Galerkin system (see appendix B for details).

In this study, we develop a subgrid-turbulence representation adopting the power balance as guiding proxy but pursuing an alternative approach to cure the excess resolved power. We search for a Galerkin expansion with the same mean flow as basic mode $\boldsymbol{u}_0$ but general orthogonal modes $\tilde{\boldsymbol{u}}_i$, $i = 1, \ldots, n$:

$$\tilde{\boldsymbol{u}}^{[0..n]}(\boldsymbol{x}, t) = \boldsymbol{u}_0(\boldsymbol{x}) + \sum_{i=1}^{n} \tilde{a}_i(t)\tilde{\boldsymbol{u}}_i(\boldsymbol{x}). \tag{2.21}$$

Note that the new mode coefficients $\tilde{a}_i$ cannot be expected to be uncorrelated. In other words, the covariance matrix $\tilde{\boldsymbol{\Lambda}} = (\tilde{\lambda}_{ij})$, $\tilde{\lambda}_{ij} = \langle \tilde{a}_i \tilde{a}_j \rangle_T$ is not a diagonal matrix. The resulting Galerkin system does not change its form and the new constant, linear and quadratic system coefficients are indicated by a tilde. The resulting power balance in the new Galerkin subspace reads as follows:

$$0 = \sum_{i,j=1}^{n} \tilde{L}_{ij}\tilde{\lambda}_{ij} + \tilde{T}_<. \tag{2.22}$$

The unresolved transfer term characterizes the nonlinear energy cascade but contains also linear terms, $T_< = \sum_{i=1}^{n}\sum_{j=n+1}^{\infty} \tilde{L}_{ij}\tilde{\lambda}_{ij} + \sum_{i=1}^{n}\sum_{\substack{j,k=1 \\ \max(j,k)>n}}^{\infty} \tilde{Q}_{ijk}\langle \tilde{a}_i \tilde{a}_j \tilde{a}_k \rangle_T$. The key idea is to 'rotate' the new modes $\tilde{\boldsymbol{u}}_i$ a 'minimal amount' away from the POD modes $\boldsymbol{u}_i$ into 'more dissipative regimes', so that the transfer term $\tilde{T}_< = 0$ vanishes.

Up to now, the mode coefficients a_i and $\tilde{a}_i$ have been assumed to arise from the exact Navier–Stokes solution. The Galerkin solution, however, cannot be expected to match the Navier–Stokes solution exactly. In fact, the inter-model energy flows in

Galerkin systems are often under-predicted. Hence, we introduce a free transfer term parameter ϵ, to account for such discrepancies:

$$\epsilon = \sum_{i,j=1}^{n} \tilde{L}_{ij}\tilde{\lambda}_{ij}. \tag{2.23}$$

In the following section, the sketched MOR approach is detailed.

3. Galerkin MOR approach with power balance constraint

3.1. *Formulation of a new optimization principle for the expansion modes*

In this section, a new MOR approach for high-Reynolds-number Navier–Stokes fluid flows is proposed. Instead of modelling the unresolved scales on the Galerkin system level using an eddy-viscosity term, the unresolved scales are included at the kinematic level, i.e. at the modal level. In other words, we seek a new set of spatial and temporal basis functions $\tilde{\boldsymbol{u}}_i$ and $\tilde{a}_i$ such that, in addition to optimally representing the data, they also satisfy the power balance

$$\begin{aligned} \underset{\tilde{a},\tilde{u}}{\arg\min} \quad & \left\langle \int_{\Omega} \left| \boldsymbol{u}(\boldsymbol{x},t) - \boldsymbol{u}_0(\boldsymbol{x}) - \sum_{i=1}^{n} \tilde{a}_i(t)\tilde{\boldsymbol{u}}_i(\boldsymbol{x}) \right|^2 \mathrm{d}x \right\rangle_T, \\ \text{s.t.} \quad & (1) \quad \left(\tilde{\boldsymbol{u}}_i, \tilde{\boldsymbol{u}}_j\right)_{\Omega} = \delta_{ij}, \\ & (2) \quad \sum_{i,j=1}^{n} \tilde{L}_{ij}\tilde{\lambda}_{ij} = \epsilon. \end{aligned} \tag{3.1}$$

In the spirit of related previous work (Amsallem & Farhat 2011), we propose the following parametrization of the solution to (3.1). We seek a linear transformation, from a larger subspace of POD basis functions that satisfies (3.1). One can write

$$\tilde{\boldsymbol{u}}_i = \sum_{j=1}^{N} X_{ji}\boldsymbol{u}_j, \tag{3.2a}$$

$$\tilde{a}_i = \sum_{j=1}^{N} X_{ji}a_j, \tag{3.2b}$$

where $\boldsymbol{X} \in \mathbb{R}^{N\times n}$ is an orthonormal ($\boldsymbol{X}^{\mathrm{T}}\boldsymbol{X} = I_{n\times n}$) transformation matrix and, by construction, $N > n$. The new Galerkin system tensors can be all expressed as a function of the transformation matrix $\boldsymbol{X}$ as follows:

$$\tilde{Q}_{ijk} = \sum_{p,q,r=1}^{N} X_{pi}Q_{pqr}X_{qj}X_{rk} \quad i,j,k = 1,\ldots,n, \tag{3.3a}$$

$$\tilde{\boldsymbol{L}} = \boldsymbol{X}^{\mathrm{T}}\boldsymbol{L}\boldsymbol{X}, \tag{3.3b}$$

$$\tilde{\boldsymbol{C}} = \boldsymbol{X}^{\mathrm{T}}\boldsymbol{C}, \tag{3.3c}$$

$$\tilde{\boldsymbol{\Lambda}} = \boldsymbol{X}^{\mathrm{T}}\boldsymbol{\Lambda}\boldsymbol{X}, \tag{3.3d}$$

where $\boldsymbol{C} \in \mathbb{R}^{N}, \boldsymbol{L} \in \mathbb{R}^{N\times N}$ and $\boldsymbol{Q} \in \mathbb{R}^{N\times N\times N}$ are the Galerkin system coefficients corresponding to POD modes $\boldsymbol{u}_i$ for $i = 1,\ldots,N$. Note that the transformed Galerkin

tensor $\tilde{\boldsymbol{Q}}$ remains energy conserving due to the orthonormal transformation and thus does not contribute to the energy budget. As a final step, the objective function is reformulated. The objective function in problem (3.1) is a measure of the distance between the snapshot solution $\boldsymbol{u}(\boldsymbol{x}, t)$ and the Galerkin expansion $\sum_{i=1}^{n} \tilde{a}_i(t)\tilde{\boldsymbol{u}}_i(x)$ in the energy norm. By definition, the reconstruction of the snapshot solution using POD basis functions, $\sum_{i=1}^{n} a_i(t)\boldsymbol{u}_i(x)$, is the optimal reconstruction. In other words, the following inequalities always hold:

$$\left\langle \int_{\Omega} |\boldsymbol{u}(\boldsymbol{x}, t) - \boldsymbol{u}_0(\boldsymbol{x})|^2 \, \mathrm{d}\boldsymbol{x} \right\rangle_T \geqslant \sum_{i=1}^{n} \lambda_i \geqslant \sum_{i=1}^{n} \tilde{\lambda}_i. \tag{3.4}$$

And so, the minimization problem (3.1) takes the following final form:

$$\begin{aligned} \underset{\boldsymbol{X} \in \mathbb{R}^{N \times n}}{\arg\min} \quad & \sum_{i=1}^{n} \left(\lambda_i - \left(\boldsymbol{X}^{\mathrm{T}} \boldsymbol{\Lambda} \boldsymbol{X} \right)_{ii} \right) \\ \text{s.t.} \quad & (1) \quad \boldsymbol{X}^{\mathrm{T}} \boldsymbol{X} = I_{n \times n} \\ & (2) \quad \sum_{i,j=1}^{n} \left(\boldsymbol{X}^{\mathrm{T}} \boldsymbol{L} \boldsymbol{X} \right)_{ij} \left(\boldsymbol{X}^{\mathrm{T}} \boldsymbol{\Lambda} \boldsymbol{X} \right)_{ij} = \epsilon. \end{aligned} \tag{3.5}$$

3.2. *The algorithm and numerical implementation*

For reasonably small problems, our proposed approach can be directly implemented and solved in MATLAB. Specifically, (3.5) can be solved using MATLAB's sequential quadratic programming (SQP) (Dixon & Szegö 1975; Schittkowski 1986; Nocedal & Wright 1999) implementation, `fmincon`, and the critical transfer term parameter can be found using MATLAB's Brent's method (Brent 2002) implementation, `fzero`. The entire algorithm is initialized using the time-averaged total power of the POD modes, i.e. $\epsilon = \sum_{i,j=1}^{n} L_{ij}\lambda_i$, as the initial guess for the critical transfer term parameter. Following a single solution of (3.5) using `fmincon`, the new Galerkin ROM is integrated in time and the transfer term parameter is updated using `fzero`, where the function whose root we seek is the Galerkin ROM error

$$r(\epsilon) := \sum_{i=1}^{n} \tilde{\lambda}_{ii} - \left\langle \sum_{i=1}^{n} \tilde{a}_i^2(t) \right\rangle_T. \tag{3.6}$$

The mode coefficients $\tilde{a}_i$ in (3.6) are those derived from a numerical integration of the corresponding new Galerkin ROM. Unfortunately, our approach does not guarantee roots for (3.6); nor does it guarantee feasible solutions for (3.5). However, for the specific test cases analysed, roots and feasible solutions were found for all model orders n and most 'reasonable' values of N. Specifically, we have found the best performance with transformations of dimension $N \approx 2n$. For these transformation dimensions, convergence to the critical transfer term parameter is achieved in less than 20 iterations, which – depending on the size of the ROM – equates to several minutes of total CPU time. Details of a simple MATLAB implementation are summarized in appendix A. The following pseudo-code summarizes the approach:

Algorithm 1 Stabilization Algorithm

Input: POD basis functions, $\boldsymbol{u}_i(\boldsymbol{x})$ and $a_i(t)$, for $i = 1, \ldots, N$, and the associated Galerkin tensors $\boldsymbol{C} \in \mathbb{R}^N$, $\boldsymbol{L} \in \mathbb{R}^{N\times N}$ and $\boldsymbol{Q} \in \mathbb{R}^{N\times N\times N}$. The transfer term parameter ϵ.

Output: Galerkin tensors $\tilde{\boldsymbol{C}} \in \mathbb{R}^n$, $\tilde{\boldsymbol{L}} \in \mathbb{R}^{n\times n}$ and $\tilde{\boldsymbol{Q}} \in \mathbb{R}^{n\times n\times n}$ associated with the transformed basis functions, $\tilde{\boldsymbol{u}}_i$, for $i = 1, \ldots, n$.

1: Choose $n > 0$, s.t. $N > n$.
2: Compute the POD eigenvalues, λ_i, $i = 1, \ldots, N$.
3: **while** $r(\epsilon) \neq 0$ **do**
4: Solve the minimization problem:

$$\begin{aligned} \underset{\boldsymbol{X}\in\mathbb{R}^{N\times n}}{\arg\min} \quad & \sum_{i=1}^{n} \left(\lambda_i - \left(\boldsymbol{X}^{\mathrm{T}}\boldsymbol{\Lambda}\boldsymbol{X}\right)_{ii}\right) \\ \text{s.t.} \quad & (1) \quad \boldsymbol{X}^{\mathrm{T}}\boldsymbol{X} = I_{n\times n} \\ & (2) \quad \sum_{i,j=1}^{n} \left(\boldsymbol{X}^{\mathrm{T}}\boldsymbol{L}\boldsymbol{X}\right)_{ij} \left(\boldsymbol{X}^{\mathrm{T}}\boldsymbol{\Lambda}\boldsymbol{X}\right)_{ij} = \epsilon. \end{aligned}$$

5: Evaluate $\tilde{\boldsymbol{\Lambda}}$ and the new Galerkin system tensors, $\tilde{\boldsymbol{C}}$, $\tilde{\boldsymbol{L}}$ and $\tilde{\boldsymbol{Q}}$.
6: Numerically integrate the new Galerkin ROM.
7: Update ϵ using the root-finding algorithm.
8: **end while**
9: Return $\tilde{\boldsymbol{u}}_i$, $\boldsymbol{X}$ and the new Galerkin system tensors $\tilde{\boldsymbol{C}}$, $\tilde{\boldsymbol{L}}$ and $\tilde{\boldsymbol{Q}}$.

4. Applications

4.1. *Lid-driven cavity*

The lid-driven cavity is a well-known benchmark problem used to validate fluid flow numerical schemes and reduced-order models (Cazemier, Verstappen & Veldman 1998; Shankar & Deshpande 2000; Terragni, Valero & Vega 2011). Specifically, the incompressible, two-dimensional flow inside a square cavity driven by a prescribed lid velocity, $\boldsymbol{u}_{lid} = (1 - x^2)^2$, is considered. The Reynolds number (Re) is defined with respect to the maximum velocity of the lid and the width of the cavity. The Navier–Stokes equation is discretized in space using Chebyshev polynomials. The convective nonlinearities are handled pseudospectrally and the Chebyshev coefficients are derived using the fast Fourier transform (FFT). The equations are integrated in time using a semi-implicit, second-order Euler scheme. Figure 1 is a snapshot of a statistically stationary solution at $Re_u = 3 \times 10^4$. This particular simulation was performed using a 128^2 Chebyshev grid. The computations were performed using 8 processors. The simulation is first initialized over 100 000 time steps ($\Delta t = 1 \times 10^{-3}$), which corresponds to a wall-clock run time of 6 h. The database is then generated: 50 000 iterations corresponding to 3 wall-clock hours to create 5000 snapshots.

4.1.1. *POD modes of the lid-driven cavity*

A database of 5000 DNS snapshots of the lid-driven cavity was used to find the POD modes $\boldsymbol{u}_i$. The non-dimensional time interval between each snapshot equalled 0.1. Increasing the number of snapshots or the time interval between each snapshot had no significant effect on the performance characteristics of the ROMs. The normalized turbulent kinetic energy captured by the first n POD modes is labelled $e^{[1..n]}$ and

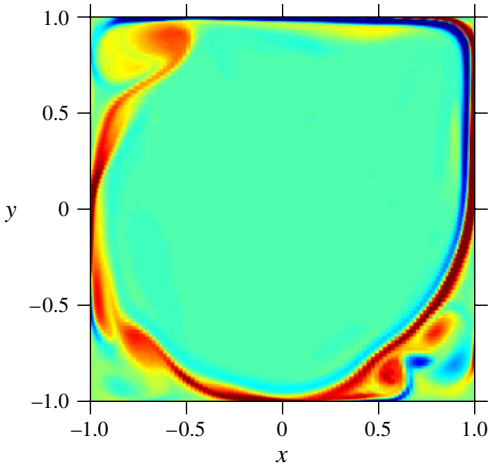

FIGURE 1. (Colour online) Vorticity contours from a DNS of the lid-driven cavity at $Re_u = 3 \times 10^4$.

n	$e^{[1..n]}$ (%)
1	16.06
2	29.21
3	37.45
4	44.88
5	50.37
10	67.16
20	82.40
50	93.21
200	99.31

TABLE 1. The normalized turbulent kinetic energy captured by the first n POD modes of the lid-driven cavity at $Re_u = 3 \times 10^4$.

defined as follows:

$$e^{[1..n]} := \frac{\langle E^{[1..n]} \rangle_T}{\langle E \rangle_T} = \frac{\sum_{i=1}^{n} \lambda_i}{\sum_{i=1}^{\infty} \lambda_i}. \tag{4.1}$$

Results for the lid-driven cavity are shown in table 1. Vorticity contours of spatial POD modes, $\boldsymbol{u}_i$, for $i = 1, 2, 20, 50$ and 200 of the lid-driven cavity, are illustrated in figure 2. As expected, the low-order POD modes correspond to the large, high-energy physical scales of the unsteady flow, while the higher-order POD modes correspond to the small, low-energy physical scales.

4.1.2. *Galerkin ROMs of lid-driven cavity using standard POD modes*

In this section, Galerkin ROMs of the lid-driven cavity are derived using the standard POD modes, $\boldsymbol{u}_i$ for $i = 1, \ldots, n$. The instantaneous turbulent kinetic energy as predicted by these ROMs is illustrated in figure 3. Numerical integration of the

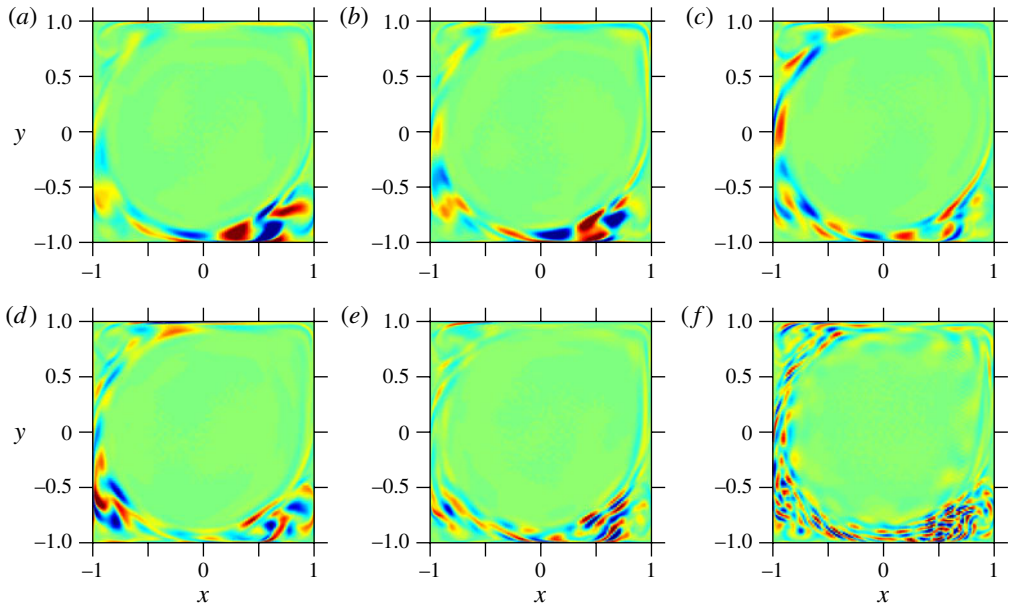

FIGURE 2. (Colour online) Vorticity contours of spatial POD modes of the lid-driven cavity at $Re_u = 3 \times 10^4$: (*a*) $\boldsymbol{u}_1$; (*b*) $\boldsymbol{u}_2$; (*c*) $\boldsymbol{u}_{10}$; (*d*) $\boldsymbol{u}_{20}$; (*e*) $\boldsymbol{u}_{50}$; (*f*) $\boldsymbol{u}_{200}$.

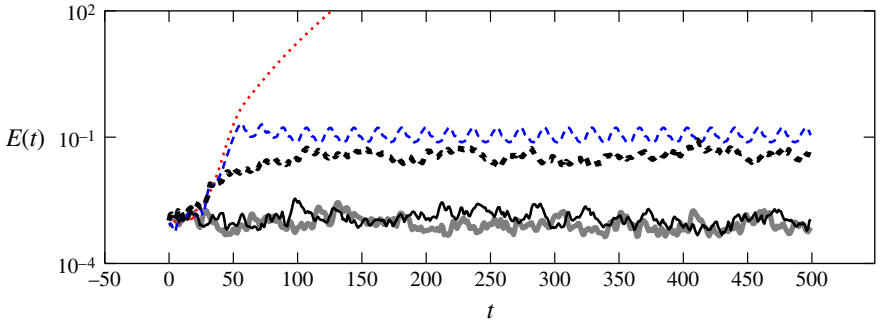

FIGURE 3. (Colour online) The evolution of the instantaneous turbulent kinetic energy of the lid-driven cavity as predicted by standard POD-based Galerkin ROMs of order $n = 5$ (dotted red line), 10 (dashed blue line), 50 (dashed black line) and 200 (solid black line); DNS (thick grey line).

ROM was performed in MATLAB, using the adaptive forth/fifth order Runge–Kutta scheme `ODE45`. Despite the fact that the POD modes capture a large normalized turbulent kinetic energy of the snapshot solution (see table 1), figure 3 clearly indicates that low-order Galerkin ROMs based on these modes do not resolve the direct numerical solution. Good agreement between ROM and DNS is achieved only when a prohibitively large number of POD modes are utilized; approximately $n = 200$ POD modes for this particular test case. These convergence issues, of course, were anticipated. Galerkin ROMs of the Navier–Stokes equation that utilize only the first few most energetic POD modes tend to under-resolve the small, energy-dissipating scales of the turbulent flow – which, therefore, leads to excessive resolved power. As discussed in § 3, the time-averaged resolved power associated with the POD modes

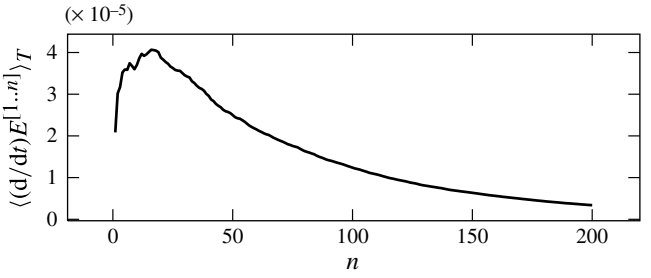

FIGURE 4. The time-averaged resolved power of the first n POD modes of the lid-driven cavity.

can be calculated using (2.23); these rates are illustrated in figure 4. As shown, the time-averaged resolved power associated with the first n POD modes is always positive and approaches zero asymptotically. It is not surprising, therefore, that ROMs derived using only the most energetic modes tend to over-predict the kinetic energy of the flow.

4.1.3. *Galerkin ROMs of lid-driven cavity using the proposed new modes*

In this section, ROMs of the lid-driven cavity are derived using the new proposed methodology. Galerkin ROMs are derived using modes with *negative* time-averaged resolved power, i.e. modes for which $\langle (\mathrm{d}/\mathrm{d}t)E^{[1..n]}\rangle_T = \epsilon < 0$. In the previous section, it was demonstrated that the standard POD basis functions have positive time-averaged resolved power, $\langle (\mathrm{d}/\mathrm{d}t)E^{[1..n]}\rangle_T = \epsilon > 0$ and therefore, produce Galerkin ROMs that over-predict the kinetic energy of the flow. The critical time-averaged resolved power ϵ for the new modes is found iteratively, using the algorithm introduced in § 3.2 using $N = 2n$.

Figure 5 illustrates the evolution of the instantaneous turbulent kinetic energy of the lid-driven cavity as predicted by the new Galerkin ROMs. For the sake of brevity, only $n = 5, 10$ and 20 ROMs are illustrated. As predicted, ROMs derived using the new modes converge to the correct mean value of kinetic energy and the accuracy of the models is improved as n is increased. Figure 6 illustrates the power spectral density (PSD) of the instantaneous turbulent kinetic energy as predicted by the new ROMs. The PSD is estimated using Welch's averaged, modified periodogram method (Welch 1967). Specifically, MATLAB's built-in Welch's algorithm, `cpsd`, is utilized. The estimation is performed using a Hamming window with a 50 % overlap. The length of the Hamming window is such that two equal sections of the signal are used to compute the average. The results in figure 6 demonstrate that the ROMs also converge to the correct attractor. As stated previously, these new modes have negative time-averaged resolved power ϵ, while the standard POD modes have positive values. Despite this difference, these new modes remain very similar to the POD modes, as summarized in table 2. The normalized turbulent kinetic energy captured by the first n new modes $\tilde{e}^{[1..n]}$ is defined by

$$\tilde{e}^{[1..n]} := \frac{\sum_{i=1}^{n} \tilde{\lambda}_{ii}}{\sum_{i=1}^{\infty} \lambda_i}. \tag{4.2}$$

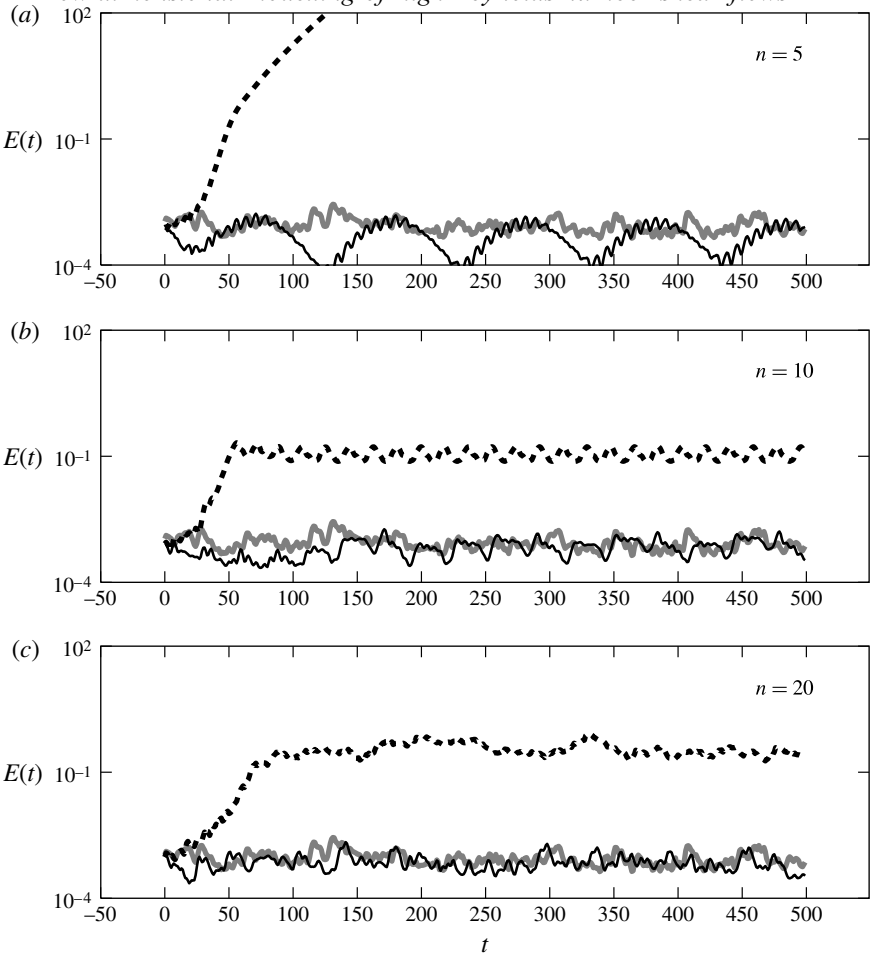

FIGURE 5. The evolution of the instantaneous turbulent kinetic energy of the lid-driven cavity as predicted by standard POD-based Galerkin ROMs (dashed black lines) and the new Galerkin ROMs (solid black lines); DNS (thick grey lines).

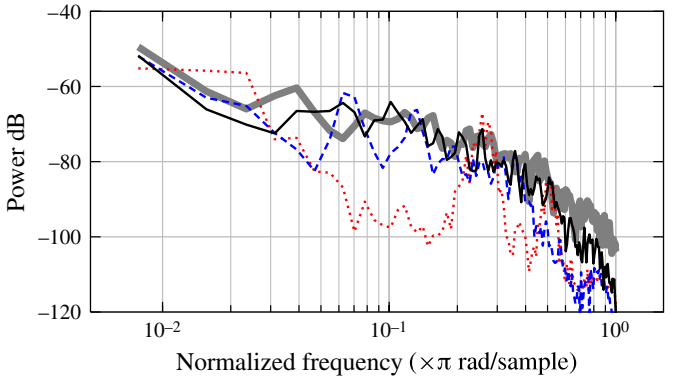

FIGURE 6. (Colour online) PSD of the turbulent kinetic energy of the lid-driven cavity as predicted by the new Galerkin ROMs of order $n = 5$ (dotted red line), 10 (dashed blue line) and 20 (thin black line); DNS (thick grey line).

n	$e^{[1..n]}$ (%)	ϵ	$\tilde{e}^{[1..n]}$ (%)	$\tilde{\epsilon}$
5	50.37	3.60×10^{-5}	50.01	-1.78×10^{-5}
10	67.16	3.70×10^{-5}	66.72	-2.22×10^{-5}
20	82.40	3.88×10^{-5}	82.11	-1.60×10^{-5}

TABLE 2. The normalized turbulent kinetic energy and time-averaged resolved power captured by the first n POD and the proposed new modes of the lid-driven cavity.

For all orders n, the new modes capture a very similar total of kinetic energy of the flow as compared to POD modes. In fact, the transformation matrix associated with these new modes makes little change to the modes: $\boldsymbol{u}_i \approx \tilde{\boldsymbol{u}}_i$. This matrix reads

$$\boldsymbol{X}_{N\times n} = \begin{bmatrix} I_{n\times n} \\ O_{(N-n)\times n} \end{bmatrix} + \delta_{N\times n}, \tag{4.3}$$

where $I_{n\times n}$ and $O_{(N-n)\times n}$ are the identity and null matrices, respectively. $\delta_{N\times n}$ is a matrix whose entries are all less than one, i.e. $|\delta_{ij}| \ll 1 \, \forall i, j$. Therefore, the new modes inherit much of the optimality of the original POD modes.

4.2. *Mixing layer*

The database used for the present work corresponds to the DNS of an isothermal two-dimensional mixing layer. The numerical algorithm is the same as that employed previously for studies on jet noise sources (Cavalieri *et al.* 2011). The full Navier–Stokes equation for two-dimensional fluid motion is formulated in Cartesian coordinates and solved in conservative form. Spatial derivatives are computed with a fourth-order-accurate finite scheme for both the inviscid and viscous portions of the flux (Gottlieb & Turkel 1976; Hayder & Turkel 1993). A second-order predictor–corrector scheme is used to advance the solution in time. In addition, block decomposition and MPI parallelization are implemented. The three-dimensional Navier–Stokes equation characteristic non-reflective boundary conditions (3D-NSCBC), developed by Lodato, Domingo & Vervisch (2008), are applied at the boundaries of the computational domain to account for convective fluxes and pressure gradients across the boundary plane. In order to simulate anechoic boundary conditions, the mesh is stretched and a dissipative term is added to the equations in the sponge zone (Colonius, Lele & Moin 1993). A detailed description of the numerical procedure is given in Daviller (2010).

The inflow mean streamwise velocity profile is given by a hyperbolic tangent profile:

$$\overline{u}(y) = U_2 + \Delta U \left[\frac{1 + \tanh(2y)}{2} \right], \tag{4.4}$$

with $\Delta U = U_1 - U_2$ being the velocity difference across the mixing layer, where U_1 and U_2 are the initial velocity above and below, respectively. The velocities, lengths and time are non-dimensionalized with ΔU and the initial vorticity thickness δ_ω. The flow Reynolds number is $Re = \delta_\omega \Delta U / \nu_a = 500$, where the subscript $(\cdot)_a$ indicates a constant ambient quantity. The Mach numbers of the free streams are $M_1 = U_1/c_a = 0.1$ and $M_2 = U_2/c_a = 0.033$, where c_a is the speed of sound. The inflow mean temperature is calculated with the Crocco–Busemann relation, and the

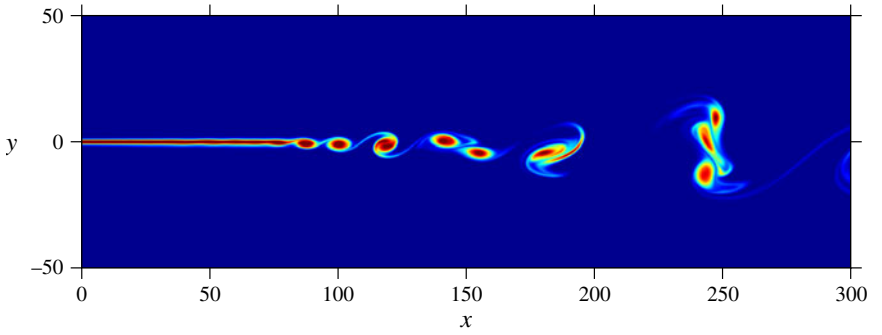

FIGURE 7. (Colour online) Vorticity contours from a DNS of the mixing at $Re_{\delta_\omega} = 500$.

n	$e^{[1..n]}$ (%)
1	18.05
2	34.69
3	40.20
4	46.23
5	50.71
10	66.80
20	81.77
50	93.93
100	98.36

TABLE 3. The normalized turbulent kinetic energy captured by the first n POD modes of the mixing layer at $Re_{\delta_\omega} = 500$.

inflow mean pressure is constant. The Prandtl number is selected to be $Pr = 0.7$. Finally, the convective Mach number is given by $M_c = \Delta U/2c_a = 0.033$, so that the flow can be assumed to be quasi-incompressible. The numerical code was extensively validated against numerical and experimental data; some results can be found in Daviller (2010) and Cavalieri *et al.* (2011).

The computations were performed on the cluster of the PPRIME Institute, using 64 processors. The computational domain comprises approximately 2.1 million grid points: 2367 points in the streamwise direction and 884 points along the y direction. The extension of the computational domain is $325\delta_\omega \times 120\delta_\omega$. The sponge regions are from $x = -20\delta_\omega$ to $x = 0$ and $x = 250\delta_\omega$ to $x = 305\delta_\omega$ in the streamwise direction, and from $\pm 50\delta_\omega$ to $\pm 60\delta_\omega$ in the transverse y direction. To promote a natural transition to turbulence from an initially laminar solution, the flow is forced by adding at every iteration solenoidal perturbations defined as in Bogey (2000). The simulation is first initialized over 330 000 time steps ($\Delta t = 0.002$), which corresponds to a wall-clock run time of 35 h. The database is then generated: 1 093 695 iterations corresponding to 115 wall-clock hours to create 2000 snapshots.

4.2.1. *POD modes of the mixing layer*

A database of 2000 DNS snapshots of the mixing-layer cavity were used to find the POD modes $\boldsymbol{u}_i$. The non-dimensional time interval between each snapshot equals unity. Increasing the number of snapshots or the time interval between each snapshot had

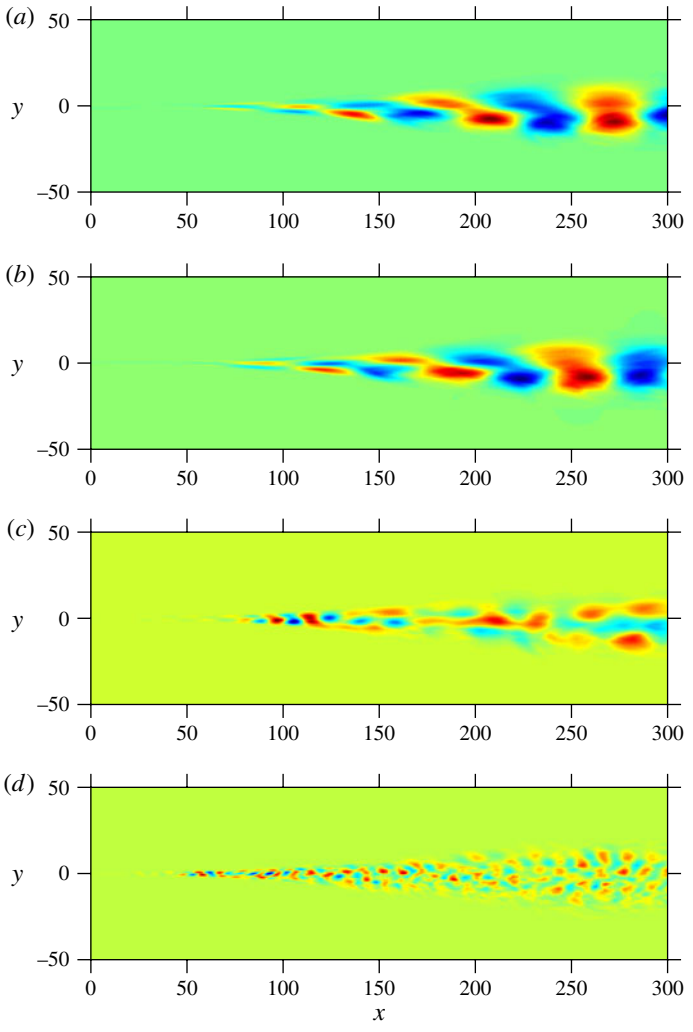

FIGURE 8. (Colour online) Vorticity contours of spatial POD modes of the mixing layer at $Re_{\delta_\omega} = 500$: (*a*) $\boldsymbol{u}_1$; (*b*) $\boldsymbol{u}_2$; (*c*) $\boldsymbol{u}_{20}$; (*d*) $\boldsymbol{u}_{100}$.

no noticeable effect on the performance characteristics of the ROMs. The percentages of time-averaged, turbulent kinetic energy captured by the first n POD modes of the mixing layer are summarized in table 1. Vorticity contours of spatial POD modes, $\boldsymbol{u}_i$, for $i = 1, 2, 20$ and 100, of the mixing layer are illustrated in figure 8. As before, the low-order POD modes correspond to the large, high-energy physical scales of the unsteady flow, while the higher-order POD modes correspond to the small, low-energy physical scales.

4.2.2. *Galerkin ROMs of the mixing layer using standard POD modes*

In this section, Galerkin ROMs of the mixing layer are derived using standard POD modes $\boldsymbol{u}_i$ for $i = 1, \ldots, n$. The turbulent kinetic energy as predicted by these ROMs is illustrated in figure 9. Similar to the lid-driven cavity test case, Galerkin ROMs of the mixing layer based on POD modes over-predict the kinetic energy of the flow.

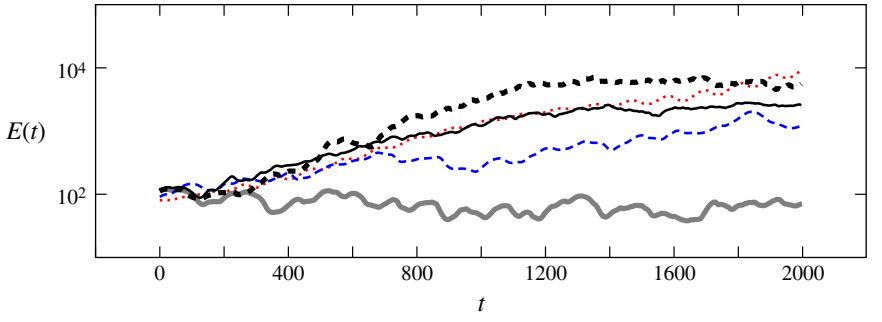

FIGURE 9. (Colour online) The evolution of the instantaneous turbulent kinetic energy of the mixing layer as predicted by standard POD-based Galerkin ROMs of order $n = 5$ (dotted red line), 10 (dashed blue line), 50 (thick dashed black line) and 100 (solid black line); DNS (thick grey line).

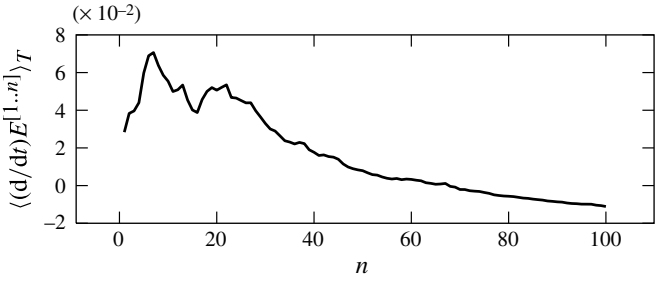

FIGURE 10. The time-averaged resolved power of the first n POD modes of the mixing layer.

These inaccuracies were anticipated because the time-averaged power resolved power associated with the POD modes is positive (see figure 10).

4.2.3. *Galerkin ROMs of the mixing layer using the proposed new modes*

In this section, the proposed new methodology is used to derive more accurate Galerkin ROMs of the mixing layer. Figure 11 illustrates the evolution of the turbulent kinetic energy of the mixing layer as predicted by the new Galerkin ROMs. For the sake of brevity, only $n = 5$, 10 and 20 ROMs are illustrated. The critical rate of the time-averaged resolved power ϵ for each ROM order n was found iteratively using the algorithm introduced in § 3.2, using $N = 2n$. As expected, the new Galerkin ROMs converge to the correct mean of kinetic energy of the DNS. Finally, figure 12 illustrates that the new ROMs also converge to the correct attractor. As stated previously, these new modes have negative time-averaged resolved power $\epsilon < 0$, while the standard POD modes have positive values. Despite this difference, these new modes remain very similar to the POD modes, as summarized in table 4.

5. Conclusions and future directions

The starting point of this study is the POD–Galerkin method, which yields a modal expansion on a kinematic level and a dynamical system as a Navier–Stokes equation surrogate. We have generalized this method to account for constraints from the Navier–Stokes equation already at the kinematic level. Traditionally, the modal

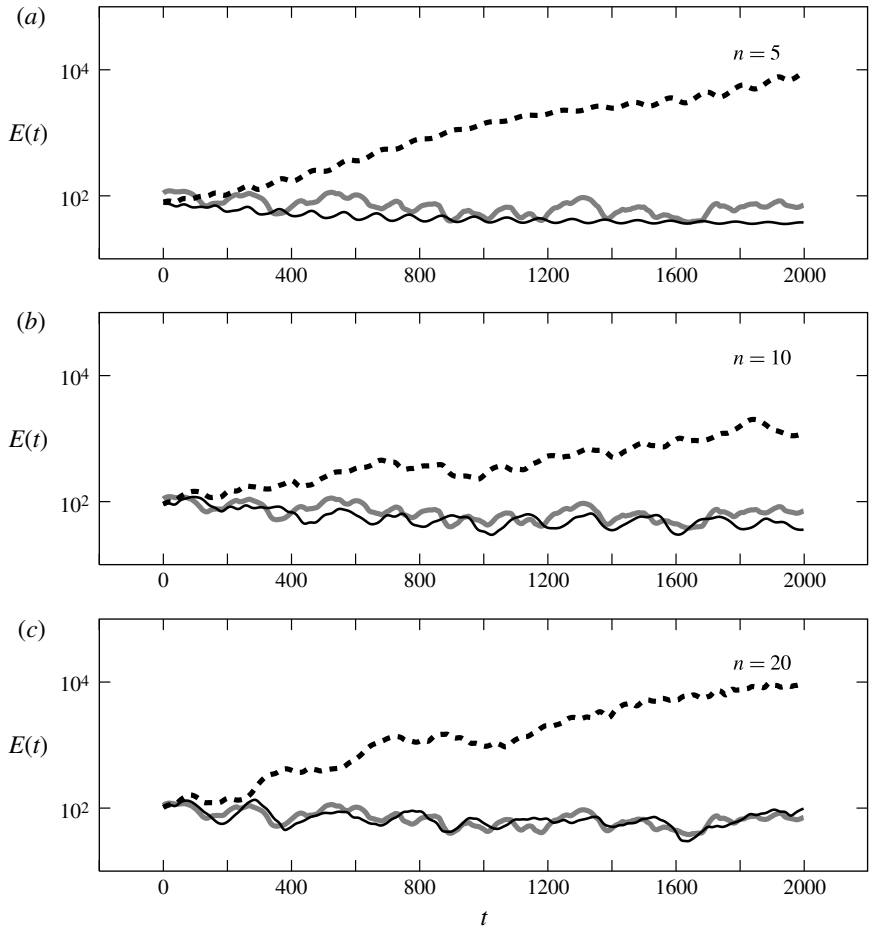

FIGURE 11. The evolution of the instantaneous turbulent kinetic energy of the mixing layer as predicted by standard POD-based Galerkin ROMs (dashed black lines) and the new Galerkin ROMs (solid black lines); DNS (thick grey lines).

n	$e^{[1..n]}$ (%)	ϵ	$\tilde{e}^{[1..n]}$ (%)	$\tilde{\epsilon}$
5	50.71	5.98×10^{-2}	50.21	-2.61×10^{-2}
10	66.80	5.54×10^{-2}	66.67	-7.52×10^{-2}
20	81.77	5.06×10^{-2}	79.14	-1.65×10^{-1}

TABLE 4. The normalized turbulent kinetic energy and time-averaged resolved power captured by the first n POD and the proposed new modes of the mixing layer.

compression of flow data yields the POD expansion, which minimizes the average expansion residual for the provided data. This approach is biased towards large, energy-producing scales, as opposed towards small-scale dissipative structures. Thus, a straightforward Galerkin projection on to the Navier–Stokes equation tends to yield a Galerkin system with unbounded solutions or fluctuation levels that are too large.

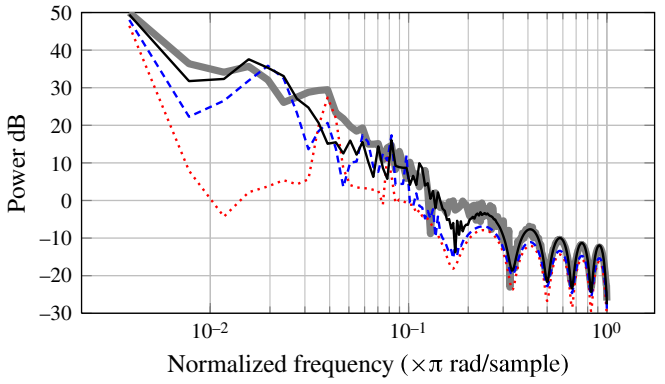

FIGURE 12. (Colour online) PSD of the turbulent kinetic energy of the mixing layer as predicted by the new Galerkin ROMs of order $n = 5$ (dotted red line), 10 (dashed blue line) and 20 (solid black line); DNS (thick grey line).

The key to a cure is the power balance for the resolved fluctuation on the attractor. Typically, the unresolved dissipative structures are accounted for by an auxiliary eddy-viscosity term in the Galerkin system, i.e. on the dynamic level. In the proposed generalization, we incorporate this power balance as a new kinematic constraint for the Galerkin expansion, thus generalizing POD. Now, the projection of the Navier–Stokes equation on to the new modal expansion satisfies the power balance on the attractor by construction. No eddy-viscosity term is needed for this purpose.

The proposed model order reduction (MOR) is employed to confined and open high-Reynolds-number flows, both of which exhibit unphysical solutions of traditional Galerkin systems based on POD without subgrid-turbulence representation. The Navier–Stokes constrained POD expansion is demonstrated to yield satisfactory Galerkin solutions after a straightforward Galerkin projection.

The traditional and new POD–Galerkin methods can be expected to converge with an increasing number of modes as the power balance will be increasing adequately resolved by the traditional POD expansion. For the targeted low-order models, the Navier–Stokes constrained POD–Galerkin method may enable a physical representation of the nonlinear energy cascade. In contrast, a linear eddy-viscosity term expressly ignores nonlinear amplitude damping. An unexplored opportunity of our approach is the inclusion of more constraints from the Navier–Stokes equation in the Galerkin expansion, e.g. the Reynolds equation.

Acknowledgements

We acknowledge financial support from the Natural Science and Engineering Research Council of Canada (NSERC) and the Chair of Excellence ‘Closed-loop control of turbulent shear flows using reduced-order models’ (TUCOROM), supported by the French Agence Nationale de la Recherche (ANR) and hosted by Institute PPRIME. We also thank Ambrosys Ltd. (Society for Complex Systems Management) and the Bernd Noack Cybernetics Foundation for additional support. We appreciate the valuable and stimulating discussions with C. Farhat and D. Amsallem at Stanford University and J.-P. Bonnet, L. Cordier, J. Delville and V. Parezanovic from the Institute PPRIME. We are particularly grateful to G. Daviller (now at CERFACS, Toulouse, France) for making the mixing-layer dataset available to us. We also thank

N. Maamar for a wonderful job in accommodating the intensive TUCOROM visitor programme at Institut PPRIME.

Appendix A. MATLAB implementation

The following is a simple MATLAB implementation of the proposed Navier–Stokes constrained POD algorithm. The inputs of the function `constrained_POD` are the POD temporal coefficients `a`, the linear Galerkin matrix $\boldsymbol{L}$, the transformation dimensions `N` and `n`, and the transfer term parameter `epsilon`. The output of this function is the transformation matrix, $\boldsymbol{X}$. The objective function `objective` evaluates the difference between the optimal reconstruction of the time-averaged, turbulent kinetic energy using the POD basis functions and the new basis functions. The constraint function `constraint` evaluates the time-averaged resolved power for a given `epsilon`.

```
function [X] = constrained_POD(a,L,N,n,epsilon)
    global lambda L epsilon

    for i=1:N;
        lambda(i) = mean(a(i,:).*a(i,:));
    end

    x0 = eye(n,n);
    x0(N,:) = 0;

    problem = createOptimProblem('fmincon', ...
                'objective', @objective, ...
                'nonlcon', @constraint, ...
                'x0',x0);
    [x,fval,EXITFLAG,OUTPUT,LAMBDA] = fmincon(problem)
    OUTPUT.message

    X = x*(x'*x)^(-1/2);
end
```

```
function [f] = objective(x)
global lambda;
    X = x*(x'*x)^(-1/2);
    sum_lambda = sum(lambda);
    lambda_tilde = diag(X'*diag(lambda)*X);
    sum_lambda_tilde = sum(lambda_tilde);

  f = (sum_lambda - sum_lambda_tilde)/sum_lambda;
end
```

```
function [c,ceq] = constraint(x)
global L lambda epsilon;
    X = x*(x'*x)^(-1/2);
    L_tilde = X'*L*X;
    lambda_tilde = (X'*diag(lambda)*X);
    ceq = sum(sum(L_tilde.*lambda_tilde)) - epsilon;
    c = [];
end
```

Tables 5 and 6 summarize the computational costs and online ROM speed-ups for the lid-driven and mixing-layer test cases, respectively. The CFD wall-clock hours for the lid-driven cavity and mixing layer equalled 3 and 115 h, respectively. The ROM

n	Solving for ϵ	ROM	Online speed-up
5	9.8×10^{-4}	6.5×10^{-5}	4.6×10^{4}
10	6.0×10^{-2}	6.6×10^{-5}	4.5×10^{4}
20	1.8×10^{-1}	4.4×10^{-4}	6.8×10^{3}

TABLE 5. A summary of the computational costs (in wall-clock hours) and online ROM speed-ups for the lid-driven cavity.

n	Solving for ϵ	ROM	Online speed-up
5	9.4×10^{-3}	1.0×10^{-6}	1.2×10^{8}
10	8.0×10^{-2}	1.9×10^{-6}	6.1×10^{7}
20	8.3×10^{-2}	5.0×10^{-5}	2.3×10^{6}

TABLE 6. A summary of the computational costs (in wall-clock hours) and online ROM speed-ups for the mixing layer.

online speed-up is defined as the CFD wall-clock hours divided by ROM wall-clock hours.

Appendix B. Important similarities with previous approaches

The proposed approach shares important theoretical and practical aspects with subgrid-turbulence representations of Galerkin models in the literature. Virtually all representations employ the power balance equation as a proxy and add in some form of additional dissipation as a stabilizer. The first pioneering POD–Galerkin model by Aubry *et al.* (1988) contains a single additional eddy-viscosity parameter. Its value is determined by a solution-matching procedure. However, with a single effective viscosity, the turbulent coherent structure model can be derived from a projection on the low-Reynolds-number Navier–Stokes equation, i.e. this ansatz is a strong imposition (Rempfer & Fasel 1994) for the calibration of these viscosities. This approach has been successfully employed up to the present day. A corresponding application to the lid-driven cavity has been presented by Cazemier *et al.* (1998). An even more general ansatz is the identification of an additional linear term in the Galerkin system to account for unresolved turbulent fluctuations and other phenomena (Galletti *et al.* 2004). These authors have employed a solution-matching procedure. The advantage is the possibility of including, for instance, frequency changes due to unresolved turbulence. However, the ansatz cannot easily be physically interpreted.

The above subgrid-turbulence representations propose a linear term for a nonlinear turbulence cascade. The price is a potential – if not likely – lack of robustness of the closure. The damping at large fluctuations is generally under-predicted. Noack *et al.* (2011) have proposed a nonlinear eddy-viscosity term that is consistent with the finite-time thermodynamics closure (Noack *et al.* 2008) and that guarantees the boundedness of the Galerkin solution (Cordier *et al.* 2013). Borggaard's group pursues a similar goal of more realistic nonlinear subgrid-turbulence representations. They derive nonlinear terms from a Galerkin projection of an LES-filtered Navier–Stokes equation (Wang *et al.* 2011, 2012).

The need for a subgrid-turbulence closure model rests in a property of POD. By construction, POD is biased towards the large, energy-containing scales of the turbulent flow. In fact, Lumnley (1967) has introduced POD with the very purpose of distilling just the coherent flow structures. There have been several previous attempts at generalizing POD in the past. For example, Iollo, Lanteri & Désidéri (2000) formulate the POD with respect to the Sobolev H^1 norm. The inclusion of derivatives of the snapshot matrix increases the contribution of the small scales of the turbulent flow in the basis functions and, therefore, tends to stabilize the Galerkin ROMs. The price is an empirical calibration of the exact definition of the Sobolev norm to achieve stability.

In the proposed new approach, we comprise several constitute elements of the above approaches. Similarly to Iollo *et al.* (2000), we have generalized the POD algorithm so that a more appropriate balance of large and small scales is included in the basis functions. Similarly to Cazemier *et al.* (1998), we utilize the power balance equation derived from the Navier–Stokes equation as an additional constraint. Following Noack *et al.* (2011) and Wang *et al.* (2011), we respect the nonlinear energy transfer by allowing the reduced-order model to establish its own nonlinear energy transfer from producing to dissipative modes. Conceptually, one might consider the proposed new ROM as a POD ROM enriched with additional energy-absorbing dynamic equations, as opposed to an additional energy-absorbing term.

REFERENCES

Amsallem, D. & Farhat, C. 2011 Stabilization of projection-based reduced-order models. *Intl J. Numer. Meth. Engng* **91** (4), 358–377.

Aubry, N., Holmes, P., Lumley, J. L. & Stone, E. 1988 The dynamics of coherent structures in the wall region of a turbulent boundary layer. *J. Fluid Mech.* **192** (115), 115–173.

Bailon-Cuba, J., Shishkina, O., Wagner, C. & Schumacher, J. 2012 Low-dimensional model of turbulent mixed convection in a complex domain. *Phys. Fluids* **24**, 107101.

Bogey, C. 2000 Calcul direct du bruit aérodynamique et validation de modèles acoustiques hybrides. PhD thesis, Ecole Centrale Lyon, France.

Boyd, J. P. 2001 *Chebyshev and Fourier Spectral Methods*, 2nd edn. Dover.

Brent, R. P. 2002 *Algorithms for Minimization without Derivatives*. Dover.

Canuto, C., Hussaini, M. Y., Quarteroni, A. & Zang, T. A. 1991 *Spectral Methods in Fluid Dynamics*. Springer.

Canuto, C., Hussaini, M. Y., Quarteroni, A. & Zang, T. A. 2006 *Spectral Methods: Fundamentals in Single Domains*. Springer.

Cavalieri, A., Daviller, G., Comte, P., Jordan, P., Tadmor, G. & Gervais, Y. 2011 Using large eddy simulation to explore sound-source mechanisms in jets. *J. Sound Vib.* **330**, 4098–4113.

Cazemier, W., Verstappen, R. W. C. P. & Veldman, A. E. P. 1998 Proper orthogonal decomposition and low-dimensional models for driven cavity flows. *Phys. Fluids* **10** (7), 1685–1699.

Colonius, T., Lele, S. K. & Moin, P. 1993 Direct computation of the sound generated by two-dimensional shear layer. In *15th AIAA Aeroacoustics Conference*. Long Beach.

Cordier, L., Noack, B. R., Daviller, G., Delville, J., Lehnasch, G., Tissot, G., Balajewicz, M. & Niven, R. K. 2013 Control-oriented model identification strategy. *Exp. Fluids* (submitted).

Daviller, W. 2010 Numerical study of temperature effects in single and coaxial jets. PhD thesis, École Nationale Supérieure de Mécanique et d'Aérotechnique (ENSMA), Poitiers, France.

Demmel, J. W. 1997 *Applied Numerical Linear Algebra*. SIAM.

Dixon, L. C. W. & Szegö, G. P. 1975 *Towards Global Optimisation: Proceedings of a Workshop at the University of Cagliari, Italy, October 1974*. North Holland.

FLETCHER, C. A. J. 1984 *Computational Galerkin Methods*. Springer.

GALLETTI, B., BRUNEAU, C. H., ZANNETTI, L. & IOLLO, A. 2004 Low-order modelling of laminar flow regimes past a confined square cylinder. *J. Fluid Mech.* **503**, 161–170.

GOTTLIEB, D. & TURKEL, E. 1976 Dissipative two–four method for time dependent problems. *Maths Comput.* **30** (136), 703–723.

HAYDER, M. E. & TURKEL, E. 1993 High-order accurate solutions of viscous problem. In *AIAA paper* 93-3074.

HOLMES, P., LUMLEY, J. L., BERKOOZ, G. & ROWLEY, C. W. 2012 *Turbulence, Coherent Structures, Dynamical Systems and Symmetry*, 2nd edn. Cambridge University Press.

ILIESCU, T. & WANG, Z. 2012 Variational multiscale proper orthogonal decomposition: Navier–Stokes equations. Preprint arXiv: 1210.7389.

IOLLO, A., LANTERI, S. & DÉSIDÉRI, J.-A. 2000 Stability properties of Pod–Galerkin approximations for the compressible Navier–Stokes equations. *Theor. Comput. Fluid Dyn.* **13** (6), 377–396.

JOSEPH, D. D. 1976 *Stability of Fluid Motions, I and II*. New York, Springer-Verlag.

KRAICHNAN, R. H. & CHEN, S. 1989 Is there a statistical mechanics of turbulence? *Physica* D: *Nonlinear Phenomena* **37** (1–3), 160–172.

LADYZHENSKAYA, O. A. 1963 *The Mathematical Theory of Viscous Incompressible Flow*. Gordon & Breach.

LODATO, G., DOMINGO, P. & VERVISCH, L. 2008 Three-dimensional boundary conditions for direct and large-eddy simulation of compressible viscous flows. *J. Comput. Phys.* **227** (10), 5105–5143.

LUMNLEY, J. 1967 The structure of inhomogeneous turbulent flows. In *Atmospheric Turbulence and Wave Propagation* (ed. A. M. Yaglom & V. I. Tatarski), pp. 166–178. Nauka.

MOIN, P. & MAHESH, K. 1998 Direct numerical simulation: a tool in turbulence research. *Annu. Rev. Fluid Mech.* **30**, 539–578.

NOACK, B. R. & ECKELMANN, H. 1994 A global stability analysis of the steady and periodic cylinder wake. *J. Fluid Mech.* **270**, 297–330.

NOACK, B. R., MORZYNSKI, M. & TADMOR, G. 2011 *Reduced-Order Modelling for Flow Control*. Springer.

NOACK, B. R., PAPAS, P. & MONKEWITZ, P. A. 2005 The need for a pressure-term representation in empirical Galerkin models of incompressible shear flows. *J. Fluid Mech.* **523** (1), 339–365.

NOACK, B. R., SCHLEGEL, M., AHLBORN, B., MUTSCHKE, G., MORZYŃSKI, M., COMTE, P. & TADMOR, G. 2008 A finite-time thermodynamics of unsteady fluid flows. *J. Non-Equilib. Thermodyn.* **33** (2), 103–148.

NOCEDAL, J. & WRIGHT, S. J. 1999 *Numerical Optimization*. Springer.

POPE, S. B. 2000 *Turbulent Flows*, 6th edn. Cambridge University Press.

REMPFER, D. & FASEL, H. F. 1994 Dynamics of three-dimensional coherent structures in a flat-plate boundary layer. *J. Fluid Mech.* **275**, 257–284.

ROWLEY, C. W., MEZIC, I., BAGHERI, S., SCHLATTER, P. & HENNINGSON, D. S. 2009 Spectral analysis of nonlinear flows. *J. Fluid Mech.* **641**, 115–127.

SCHITTKOWSKI, K. 1986 NLPQL: a FORTRAN subroutine solving constrained nonlinear programming problems. *Ann. Oper. Res.* **5** (1), 485–500.

SCHMID, P. J. 2010 Dynamic mode decomposition of numerical and experimental data. *J. Fluid Mech.* **656**, 5–28.

SHANKAR, P. N. & DESHPANDE, M. D. 2000 Fluid mechanics in the driven cavity. *Annu. Rev. Fluid Mech.* **32** (1), 93–136.

SIRISUP, S. & KARNIADAKIS, G. E. 2004 A spectral viscosity method for correcting the long-term behavior of POD models. *J. Comput. Phys.* **194** (1), 92–116.

SIROVICH, L. 1987 Turbulence and the dynamics of coherent structures, Part I: coherent structures. *Q. Appl. Maths* **45**, 561–571.

TENNEKES, H. & LUMLEY, J. L. 1972 *A First Course in Turbulence*. The MIT Press.

TERRAGNI, F., VALERO, E. & VEGA, J. M. 2011 Local POD plus Galerkin projection in the unsteady lid-driven cavity problem. *SIAM J. Sci. Comput.* **33** (6), 3538–3561.

UKEILEY, L., CORDIER, L., MANCEAU, R., DELVILLE, J., GLAUSER, M. & BONNET, J. P. 2001 Examination of large-scale structures in a turbulent plane mixing layer. Part 2. Dynamical systems model. *J. Fluid Mech.* **441** (1), 67–108.

WANG, Z., AKHTAR, I., BORGGAARD, J. & ILIESCU, T. 2011 Two-level discretizations of nonlinear closure models for proper orthogonal decomposition. *J. Comput. Phys.* **230**, 126–146.

WANG, Z., AKHTAR, I., BORGGAARD, J. & ILIESCU, T. 2012 Proper orthogonal decomposition closure models for turbulent flows: a numerical comparison. *Comput. Meth. Appl. Mech. Engng* **237–240**, 10–26.

WELCH, P. 1967 The use of fast Fourier transform for the estimation of power spectra: a method based on time averaging over short, modified periodograms. *IEEE Trans. Audio Electroacoust.* **15** (2), 70–73.